

PCCP

Accepted Manuscript



This is an *Accepted Manuscript*, which has been through the Royal Society of Chemistry peer review process and has been accepted for publication.

Accepted Manuscripts are published online shortly after acceptance, before technical editing, formatting and proof reading. Using this free service, authors can make their results available to the community, in citable form, before we publish the edited article. We will replace this *Accepted Manuscript* with the edited and formatted *Advance Article* as soon as it is available.

You can find more information about *Accepted Manuscripts* in the [Information for Authors](#).

Please note that technical editing may introduce minor changes to the text and/or graphics, which may alter content. The journal's standard [Terms & Conditions](#) and the [Ethical guidelines](#) still apply. In no event shall the Royal Society of Chemistry be held responsible for any errors or omissions in this *Accepted Manuscript* or any consequences arising from the use of any information it contains.



Journal Name

ARTICLE

Improved Electron Transport Property of n-Type Naphthalenediimide Polymers through Refined Molecular Ordering and Orientation Induced by Processing Solvents

Yujin An^{a,§}, Dang Xuan Long^{b,§}, Yiho Kim^a, Yong-Young Noh^{b,*}, Changduk Yang^{a,*}

Received 00th January 20xx,
Accepted 00th January 20xx

DOI: 10.1039/x0xx00000x

www.rsc.org/

To determine the role played by the choice of processing solvent in governing photophysics, microstructure, and charge carrier transport in naphthalenediimide (NDI)-based polymers, we have prepared two new NDI-bithiophene (T2)- and NDI-thienothiophene (TTh)-containing polymers with hybrid siloxane pentyl chains (SiC₅) (P(NDI2SiC₅-T2) and P(NDI2SiC₅-TTh)). Among the various processing solvents studied here, the films prepared using chloroform exhibited far better electron mobilities ($0.16 \pm 0.1 - 0.21 \pm 0.05 \text{ cm}^2/\text{V}\cdot\text{s}$) than the corresponding samples prepared from different solvents, exceeding one order of magnitude higher, indicating the significant influence of the processing solvent on the charge transport. Upon thin-film analysis by atomic force microscopy and grazing incidence X-ray diffraction, we discovered that molecular ordering and orientation are affected by the chosen processing solvent, which is responsible for the change in the transport characteristics of this class of polymers.

Introduction

Solution-processed organic field-effect transistors (OFETs) are of increasing interest owing to their potential applications in low-cost, large-area, printed organic electronics. Recently, tremendous efforts in organic semiconductors development and device optimization have been made to significantly improve OFET performance.¹⁻⁵ Until now, many top-performing *p*-type OFETs have been developed,^{4,6,7} while the area of *n*-type organic semiconductors has generally lagged behind their *p*-type counterparts in terms of device performance, material categories, and structure–property relationships.⁸⁻¹⁴

Among the few available chemical structures with suitable *n*-type properties, a breakthrough in *n*-type OFETs occurred with the development of the polymer P(NDI2OD-T2), consisting of naphthalenediimide (NDI) and bithiophene (T2), which showed unprecedented electron mobility even under ambient conditions and strong processing versatility.^{8, 15-20} In addition to the synthesis of a wide variety of NDI-based derivatives,^{12, 21-29} numerous investigations have been carried out to analyze

the microstructure of this class of polymer films, the crystalline/amorphous content ratio, and the lamellar packing, in order to rationalize the relationship between the high electron mobility and the film texture.³⁰⁻³³

Despite such thorough study exploring the correlation between molecular structure, processing, film morphology, and device performance,^{25, 34, 35} to date, it is still not known regarding how the processing solvent impacts the microstructural and charge transport characteristics of NDI-based polymers. Therefore, a detailed investigation of the processing solvent-dependent molecular packing and charge transport properties can significantly enhance the understanding of outstanding performance and charge-transport mechanism of this material family.

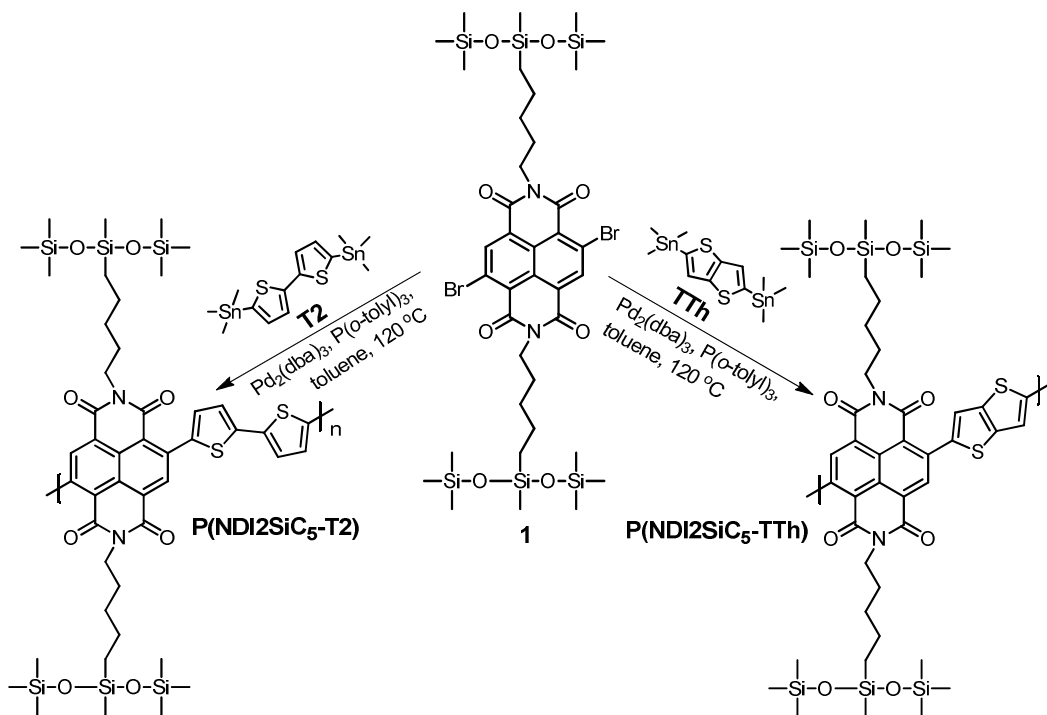
To address this relevant issue, we synthesized and characterized two new NDI-based polymers, (P(NDI2SiC₅-T2) and P(NDI2SiC₅-TTh)), comprising either T2 or thienothiophene (TTh) in an alternating fashion, in which the hybrid siloxane pentyl chains (SiC₅) as the solubilizing groups were introduced onto the repeating backbones because we were aware that the use of SiC₅ could bring relatively superior OFET properties to a certain polymer framework, based on our previous work.³⁶ Finally, we carried out spectroscopic and morphological studies, as well as OFET characterization with various processing solvents, including chloroform (CF), 1-chloronaphthalene (CN), 1,2-dichlorobenzene (DCB), and 1,1,2,2-tetrachloroethane (TCE). The electron mobilities of CF-cast films were found to be $0.21 \pm 0.05 \text{ cm}^2/\text{V}\cdot\text{s}$ for P(NDI2SiC₅-

^aDepartment of Energy Engineering, Ulsan National Institute of Science and Technology (UNIST), 50 UNIST-gil, Ulsu-gun, Ulsan, 44919, South Korea. E-mail: yang@unist.ac.kr

^bDepartment of Energy and Materials Engineering, Dongguk University, 30 Pildong-ro, 1-gil, Jung-gu, Seoul 04620, South Korea. Email: yynoh@dongguk.edu

[§]The first two authors contributed equally to this work.

Electronic Supplementary Information (ESI) available: Cyclic voltammograms, DFT data, additional AFM, and GIXD profiles. See DOI: 10.1039/x0xx00000x

Scheme 1. Synthesis of P(NDI2SiC₅-T2) and P(NDI2SiC₅-TTh)

T2) and $0.16 \pm 0.1 \text{ cm}^2/\text{V}\cdot\text{s}$ for P(NDI2SiC₅-TTh), more than one order of magnitude higher than the samples processed with other solvents. Our findings indicate that the choice of processing solvents critically influences the molecular ordering, orientation, and macroscopic charge transport efficacy.

Results and Discussion

Synthesis and Characterization: The synthetic routes for the intermediates and the polymers are shown in Scheme 1. Briefly, the key monomer *N,N'*-bis(1,1,1,3,5,5,5-heptamethyltrisiloxan-3-yl)pentyl-2,6-dibromo-1,4,5,8-naphthalenediimide (**1**) was prepared by the hydrosilylation of the pentene side chain with 1,1,1,3,5,5,5-heptamethyltrisiloxane in the presence of Karstedt's catalyst.^{6, 25, 36, 37} The palladium-catalyzed Stille polymerization of the dibrominated monomer **1** with the corresponding bistannyl comonomers (T2 and TTh) yielded P(NDI2SiC₅-T2) and P(NDI2SiC₅-TTh), respectively. Both polymers were purified by multiple Soxhlet extractions followed by dissolution-precipitation, and were then characterized by elemental analysis, ¹H NMR, and gel permeation chromatography (GPC) based on polystyrene standard in tetrahydrofuran (THF). The detailed procedures and characterizations are provided in the Experimental Section. Note that the estimated molecular weight values of the polymers only represent the THF-soluble fractions of each sample owing to their limited solubility in THF. Cyclic voltammograms of the polymer films (Figure S1) exhibited similar redox behaviors, with two reversible reduction couples and no oxidation process in the potential

range available, as observed for general NDI-based polymers.^{25, 29} The redox data are listed in Table 1. Notably, a very limited dependence of the lowest unoccupied molecular orbital (LUMO) levels on the thiophene co-monomer structures was found, which is consistent with the LUMO's preferential localization on the NDI unit.^{38, 39}

To gain insights into the role played by the processing solvents in governing the optical properties, the absorption spectra of both polymers were recorded in the solutions and as thin films using various processing solvents (CF, CN, DCB, and TCE), and the details are summarized in Table 1.

Similar to what was observed in our previous studies,^{25, 29} in all cases, there are two distinct absorption bands composed of a low-energy band attributed to the charge-transfer (CT) transition and a high-energy band arising from the $\pi-\pi^*$ transition (Figure 1). Furthermore, the spectral features of the polymers in both solutions and films strongly depend on the processing solvent, which correlates with the different aggregation as a function of the chosen processing solvent. Upon raising the temperature of the solution, we also observed a decrease in the intensities of the CT bands, implying a suppression of the pre-aggregated chain segments. Notably, the intensities of the CT bands in the films prepared from CF were observed to be higher relative to those of the corresponding films coated from other solvents, indicating a somewhat higher structural order in the CF-cast polymer films. The optical energy bandgap (E_{gap}) of P(NDI2SiC₅-T2) is smaller than that of P(NDI2SiC₅-TTh), which corroborates the enhanced electron-donating ability of T2 over TTh. The geometry-optimized structures and frontier molecular orbitals

were obtained from density functional theory (DFT) calculation at the B3LYP/6-31G* level by modeling the trimers (Figure S2).

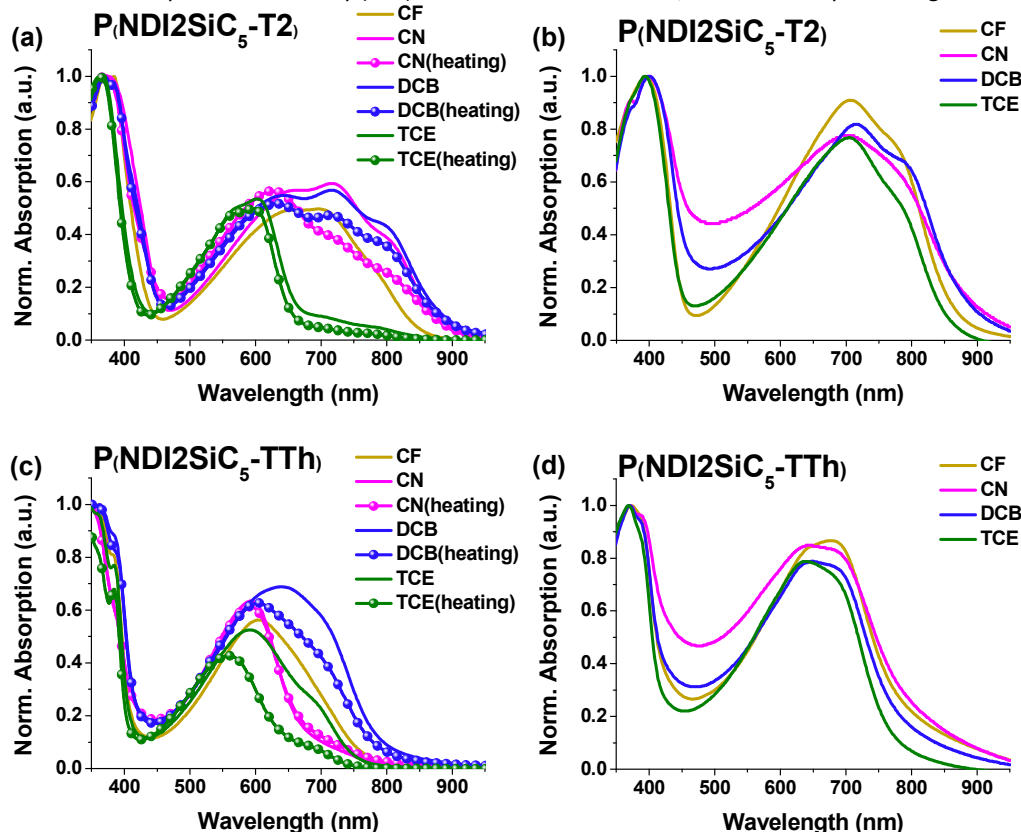


Figure 1. Absorption spectra of P(NDI2SiC₅-T2) and P(NDI2SiC₅-TTh) in solutions (a,c) and as thin films (b,d) prepared using various processing solvents.

Table 1. Optical and electrochemical properties of P(NDI2SiC₅-T2) and P(NDI2SiC₅-TTh)

Polymer	λ_{\max} soln (nm)				λ_{\max} film (nm) ^c				E_{gap} (eV) ^d	LUMO (eV) ^e	HOMO (eV) ^f
	CF	CN	DCB	TCE	CF	CN	DCB	TCE			
P(NDI2SiC ₅ -T2)	702 ^a	720 ^a	718 ^a	604 ^a	705	706	715	706	1.44	-3.80	-5.24
		628 ^b	632 ^b	599 ^b							
P(NDI2SiC ₅ -TTh)	605	594 ^a	640 ^a	592 ^a	677	643	646	639	1.57	-3.85	-5.42
		592 ^b	601 ^b	558 ^b							

^aAbsorption in solutions at 25 °C; ^bAbsorption in solutions over 80 °C; ^cAbsorption in film-state; ^dCalculated from the absorption onset in CF-cast film; ^eCyclic voltammetry determined with Fc/Fc⁺ as an internal reference (LUMO = -4.8 - ($E_{1/2\text{red}}^{\text{first}} - E_{1/2\text{ox}}^{\text{Fc/Fc}^+}$)) using thin film prepared with CF solution; ^fHOMO = LUMO - $E_{\text{g}}^{\text{opt}}$.

For both polymers, the LUMOs are mainly located around the NDI units, while the HOMOs are delocalized over the polymer backbones. An interesting point emerging from the optimized geometry is that, as in the case of other studies,^{40,41} the NDI and the thiophene-based units in the both polymers were not coplanar but showed a significant dihedral angle (θ), ranging from 43.6° to 45.4°.

Electrical Performance of OFETs: In order to unveil whether the effects of the processing solvents prevail in determining charge transport properties, as main goal in this study, top-gate, bottom-contact (TG/BC) OFETs based on both polymers were fabricated by using various solvents (CF, CN, DCB, and TCE). A dielectric layer poly(methyl-methacrylate) (PMMA) was employed in this work. The polymers (~35 nm) were deposited

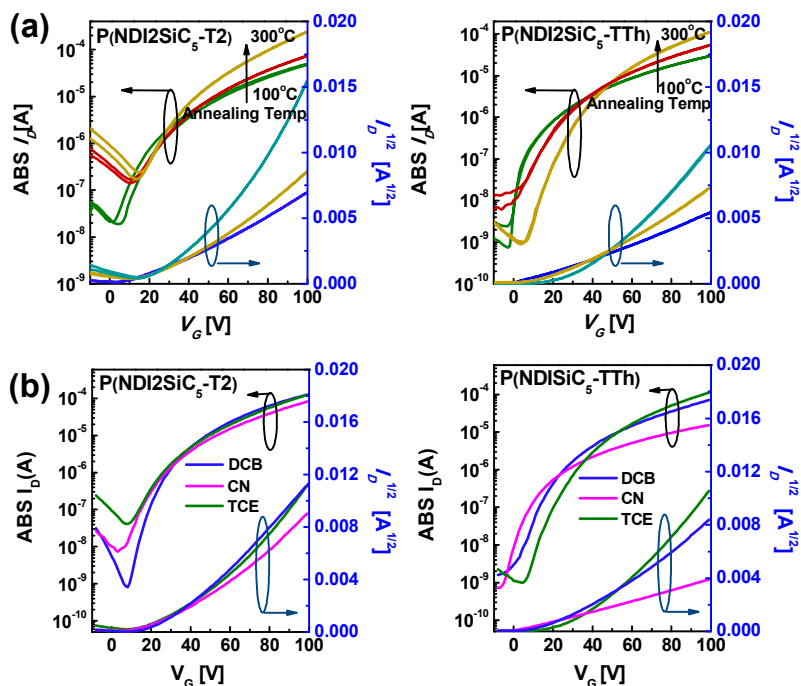


Figure 2. Transfer characteristics of the OFETs based on P(NDI2SiC₅-T2) and P(NDI2SiC₅-TTh) films prepared from CF at different annealing temperatures (a) and the films prepared using different processing solvents after annealing at 300 °C (b).

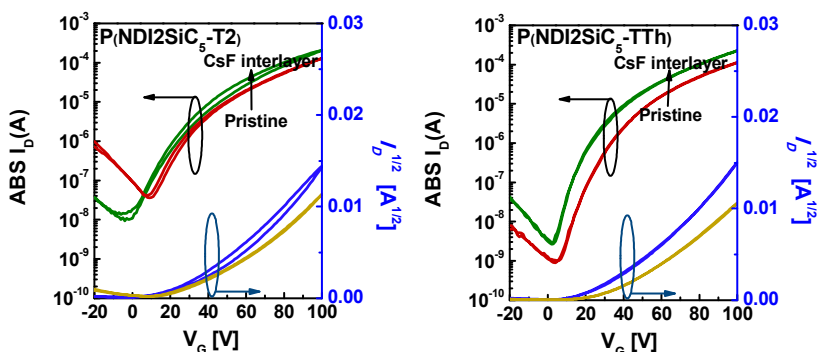


Figure 3. Transfer characteristics of the OFETs based on CF-cast P(NDI2SiC₅-T2) and P(NDI2SiC₅-TTh) films with a CsF interlayer.

by spin-coating of the polymer solutions (4 mg/mL) in each solvent.

Figure 2 shows almost ideal *n*-type transfer curves for the all devices, and the OFET parameters are listed in Table 2.

To elucidate the thermal annealing effect on OFET performance, we firstly studied each polymer film coated from CF, which was subjected to 100, 200, and 300 °C; a significant variation was observed in the electron transport behavior. The best average electron mobilities after annealing at 300 °C reached as high as 0.14 ± 0.05 cm²/V·s for P(NDI2SiC₅-T2) and 0.12 ± 0.1 cm²/V·s for P(NDI2SiC₅-TTh), respectively. Therefore, in the course of the planned study associated with the impact of the processing solvents, the films prepared from

different solvents were characterized and compared after annealing at 300 °C. For all devices, the electron mobilities of P(NDI2SiC₅-T2) are generally inferior to those of the corresponding P(NDI2SiC₅-TTh) cases. This indicates that structural change on

going from T2 to TTh in NDI-based polymers is less favorable for electron transport. Very interestingly, their OFET characteristics were found to be largely dependent on the chosen processing solvent. For example, the mobilities of P(NDI2SiC₅-T2) and P(NDI2SiC₅-TTh) films prepared from TCE were somewhat comparable to those of the corresponding CF-cast devices, whereas the use of CN for both polymers

significantly decreased their mobilities ($0.03 \pm 0.004 \sim 0.07 \pm 0.04 \text{ cm}^2/\text{V}\cdot\text{s}$) by more than one order of magnitude.

Table 2. Fundamental parameters of the OFETs based on P(NDI2SiC₅-T2) and P(NDI2SiC₅-TTh) with various processing solvents.^a

Semiconductor	Solvent/Concentration [Wt%]	Annealing temperature/Time [°C/min]	Electron mobility (μe) ($\text{cm}^2/\text{V}\cdot\text{s}$)	V_{Th} [V]	$I_{\text{on/off}}$	Contact resistance [M Ω]
P(NDI2SiC ₅ -T2)	CF/0.4	100/30	0.02 (± 0.01)	14.4	10 ⁴	143.1
		200/30	0.06 (± 0.04)	17.7	10 ³	72.6
		300/30	0.14 (± 0.05)	18.6	10 ³	39.25
	CN/0.4	200/30 (CsF interlayer)	0.21 (± 0.05)	9.4	10 ⁴	18.25
		300/30	0.07 (± 0.04)	12.7	10 ⁴	85.4
		300/30	0.12 (± 0.04)	14.6	10 ⁵	43.6
TCE/0.4	300/30	0.15 (± 0.03)	13.4	10 ³	32.5	
P(NDI2SiC ₅ -TTh)	CF/0.4	100/30	0.03 (± 0.004)	5.6	10 ⁵	140
		200/30	0.08 (± 0.007)	9.8	10 ⁴	97.6
		300/30	0.12 (± 0.1)	13.8	10 ⁵	48.2
	CN/0.4	200/30 (CsF interlayer)	0.16 (± 0.1)	9.2	10 ⁵	30.7
		300/30	0.03 (± 0.004)	9.6	10 ⁵	197.5
		300/30	0.07 (± 0.007)	8.8	10 ⁵	86.1
TCE/0.4	300/30	0.09 (± 0.01)	6.8	10 ⁴	79.4	

^aThe average mobilities of the OFET devices were measured with $L = 20 \mu\text{m}$, $W = 1000 \mu\text{m}$, and $V_D = 60 \text{ V}$. All electrical characteristics were obtained from the top-gate based transistors more than twenty devices.

The similar trend imposed by the different processing solvents was observed in previously reported work.²⁵ Therefore, one can conclude that the choice of the processing solvents is an important factor that affects the field-effect mobility in thin film transistors.

Considering the fact that CsF salt acts not only as an n -type dopant but also the electron injection is further improved with more tunneling,⁴²⁻⁴⁶ we further investigate the charge transport properties of each best-performing CF-cast device incorporating CsF interface layer between the injection electrode and the organic semiconductor (Figure 3). With this CsF layer, we are able to obtain further improved mobilities of $0.21 \pm 0.05 \text{ cm}^2/\text{V}\cdot\text{s}$ for P(NDI2SiC₅-T2) and $0.16 \pm 0.1 \text{ cm}^2/\text{V}\cdot\text{s}$ for P(NDI2SiC₅-TTh) (Table 2). Note that the CsF-applied devices were annealed at 200 °C on basis of our previous optimized process for CsF.^{42, 43}

The contact resistance (R_c) values were also extracted by using Y-function method (YFM) because the contact properties strongly affect the electrical characteristics (for details about the YFM, see the Experimental Section), and the values are also summarized in Table 2. We found that the apparent R_c values well match the trend of the mobilities obtained above, which further supports the complexity of the influence of the processing solvents on the device performance.

Thin-Film Morphology and Microstructural Order: To investigate the microstructure of the polymer films in detail with different processing solvents, we conducted atomic force microscopy (AFM) and grazing incidence X-ray diffraction

(GIXD) measurements, where the as-cast and annealed films at 300 °C were characterized.

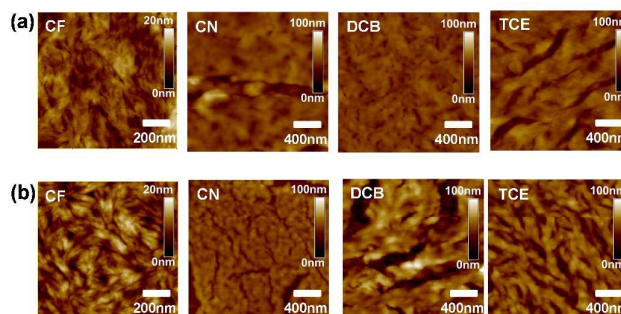


Figure 4. AFM height images of the P(NDI2SiC₅-T2) (a) and P(NDI2SiC₅-TTh) (b) annealed films at 300 °C prepared with different processing solvents.

For all the cases, together with the slightly pronounced textures after annealing compared to the corresponding as-cast films, the distinct surface morphologies in the AFM images were found to be largely dependent on the processing solvents (Figure 4 and Figure S3). To put it concretely, in contrast to other films with featureless surfaces, the both CF- and TCE-processed films after annealing were rather well-defined fibrillar structures, which most likely contribute to enhance their mobilities by hopping mechanism. We also observed that the intensities of the GIXD diffraction peaks were amplified upon annealing at 300 °C (Figure 5 and see Figure S4 and Table S1 for details of as-cast films), indicating the formation of more packed molecular conformation in the films.

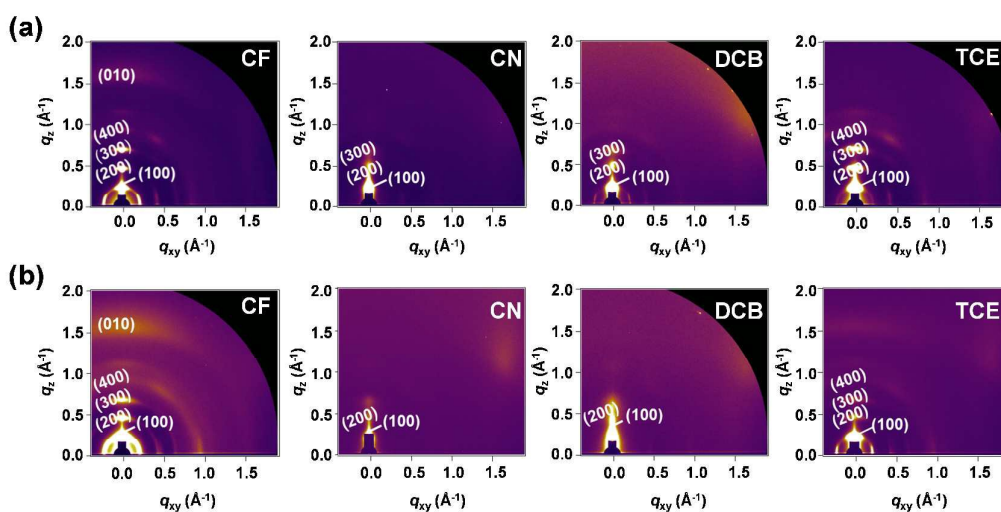


Figure 5. GIXD images of the P(NDI2SiC₅-T₂) (a) and P(NDI2SiC₅-TTh) (b) annealed films at 300 °C prepared with different processing solvents.

Table 3. Crystallographic parameters calculated from GIXD profiles of the annealing films at 300 °C.

Preparation condition	Crystallographic parameters	P(NDI2SiC ₅ -T ₂)	P(NDI2SiC ₅ -TTh)
CF	(100) q (Å ⁻¹)	0.236	0.229
	d -spacing (Å)	26.6	27.4
	π - π q (Å ⁻¹)	1.65	1.61
CN	d -spacing (Å)	3.80	3.90
	(100) q (Å ⁻¹)	0.215 ^a	0.238 ^a
	d -spacing (Å)	29.22 ^a	26.39 ^a
DCB	π - π q (Å ⁻¹)	N/A ^b	N/A ^b
	d -spacing (Å)	N/A ^b	N/A ^b
	(100) q (Å ⁻¹)	0.233	0.243 ^a
TCE	d -spacing (Å)	26.96	25.86 ^a
	π - π q (Å ⁻¹)	N/A ^b	N/A ^b
	d -spacing (Å)	N/A ^b	N/A ^b
TCE	(100) q (Å ⁻¹)	0.230	0.232
	d -spacing (Å)	27.3	27.08
	π - π q (Å ⁻¹)	N/A ^b	N/A ^b
	d -spacing (Å)	N/A ^b	N/A ^b

^aThe values were predicted from d -spacing of (200) peaks. ^bThe discernable peaks were not detected.

This observation agrees well with increase in device performance. As for the AFM images, the selection of the processing solvents has a dramatic effect on the crystallinity and molecular orientation of the both polymer films. The main findings can be summarized as follows: (i) Compared to other samples, for both polymer cases, the CF- and TCE-cast films after annealing exhibit higher ($h00$) diffraction patterns up to the fourth order along the out-of-plane (q_z) axis, signifying highly ordered lamellar structures; the lamellar d -spacing values are listed in Table 3. (ii) Notably, it is found that only the CF-cast samples yield the (010) diffraction peaks caused by π - π stacking along the q_z axis, in which the π - π stacking distances are 3.80 Å for P(NDI2SiC₅-T₂) and 3.90 Å for P(NDI2SiC₅-TTh). (iii) It is difficult to observe that any diffraction peaks are present in-plane (q_{xy} vector) for all the cases. (iv)

Consequently, the GIXD data suggest that the polymer chains in both CF and TCE-processed films are better ordered relative to the others and the CF-cast film favors a preferential face-on texture.

Conclusions

In summary, we have investigated thoroughly how the processing solvents (CF, CN, DCB, and TCE) affect the film microstructure and OFET performance of NDI-based polymers. As a model framework for this fundamental study, two NDI-based polymers (P(NDI2SiC₅-T₂) and P(NDI2SiC₅-TTh)) were designed and synthesized. We find that the use of CF can substantially improve electron transport efficiencies (0.21 ± 0.05 cm²/V·s for P(NDI2SiC₅-T₂) and 0.16 ± 0.1 cm²/V·s for

P(NDI2SiC₅-TTh)), with mobilities increasing by more than one orders of magnitude compared with the corresponding samples prepared from other solvents. The change of polymer packings and film morphologies upon the chosen processing solvent is rationalized as the main reason for the varied transport characteristics in OFETs, as evident from AFM and GIXD studies. This work advances our understanding for the role of the processing solvents on the microstructural order and charge transport properties of the NDI-based polymers.

Experimental Sections

All starting materials were purchased from Sigma-Aldrich and Acros and used without further purification. All solvents were ACS grade unless otherwise noted. ¹H NMR and ¹³C NMR spectra were recorded on a VNMRs 600 (Varian, USA) spectrophotometer using CDCl₃ as solvent and tetramethylsilane (TMS) as the internal standard. UV-Vis-NIR spectra were recorded on a UV-1800 (SHIMADZU) spectrophotometer. DFT calculations were performed using the Gaussian 09 package with the nonlocal hybrid Becke three-parameter Lee-Yang-Parr (B3LYP) function and the 6-31G* basis set to elucidate the highest occupied molecular orbital (HOMO) and LUMO levels after optimizing the geometry of P(NDI2SiC₅-T2) and P(NDI2SiC₅-TTh) using the same method. The number-average (*M_n*) and weight average (*M_w*) molecular weights, and the polydispersity index (PDI) of the polymer products were determined by GPC with a Perkin-Elmer Series 200 using a series of mono disperse polystyrene as standards in THF (HPLC grade) at 313K. Cyclic voltammetry (CV) measurements were performed on a Solartron electrochemical station (METEK, Versa STAT3) with a three-electrode cell in a 0.1 M tetra-*n*-butylammonium hexafluorophosphate (*n*-Bu₄NPF₆) solution in acetonitrile at a scan rate of 100 mV/s at room temperature. Ag/Ag⁺ (0.01M AgNO₃ in acetonitrile) electrode, a platinum wire, and a polymer-coated platinum electrode were used as the reference electrode, counter electrode, and working electrode, respectively. The Ag/Ag⁺ reference electrode was calibrated using a ferrocene/ferrocenium redox couple as an internal standard, whose oxidation potential is set at -4.8 eV with respect to zero vacuum level. The HOMO energy levels were obtained from the equation HOMO (eV) = LUMO - *E_g*^{opt}. The LUMO levels of the polymers were obtained from the equation LUMO (eV) = -4.8 - (*E*_{1/2red}^{first} - *E*_{1/2ox}^{Fe/Fc⁺}).

Synthesis of N,N'-bis(4-penten-1-yl)-2,6-dibromo-1,4,5,8-naphthalenediimide:

2,6-Dibromo-1,4,5,8-naphthalenetetracarboxylic dianhydride (3.21g, 7.53 mmol) was added to acetic acid (8 mL), and stirred for 30 min under argon. 1-Amino-4-pentene (2.08g, 24.4 mmol) was carefully added to the solution, and then heated to reflux for 24 h. The mixture was cooled to ambient temperature, and then filtered with methanol. The organic layer was dried with MgSO₄, and then concentrated under reduced pressure. The pale yellow solid product was obtained by column chromatography using CF as the eluent (1.75 g, yield 38.6%). ¹H NMR (400 MHz, CDCl₃): δ (ppm) 8.99 (s, 2H), 5.87–5.83 (m, 2H), 5.11 (s, 1H),

5.07 (s, 1H), 5.01–4.98 (d, 2H), 4.23–4.19 (m, 4H), 2.23–2.17 (m, 4H), 1.89–1.84 (m, 4H). ¹³C NMR (CDCl₃, 100 MHz): δ (ppm) 160.74, 160.71, 139.07, 137.29, 128.37, 127.72, 125.31, 124.07, 115.37, 41.14, 31.18, 26.81. Anal. Calc'd for C₂₄H₂₀Br₂N₂O₄: C, 51.45; H, 3.60; N, 5.00. Found: C, 51.38; H, 3.51; N, 5.04. MALDI-TOF MS: Calc'd for 560.23. Found: 562.04.

Synthesis of N,N'-bis(1,1,1,3,5,5,5-heptamethyltrisiloxan-3-yl)pentyl)-2,6-dibromo-1,4,5,8-naphthalenediimide (1): N,N'-Bis(4-penten-1-yl)-2,6-dibromo-1,4,5,8-naphthalenediimide (1.5 g, 2.67 mmol) and 1,1,1,3,5,5,5-heptamethylsiloxane (1.31 g, 5.89 mmol) were added to anhydrous toluene (80 mL), then Karstedt's catalyst (40 mg) was added dropwise. The reaction mixture was heated to 80 °C for 24 h, then cooled to ambient temperature, and then concentrated under reduced pressure. The pale yellow solid product was obtained by column chromatography (eluent: CF/hexane = 4/1) (0.35 g, yield 13.1%). ¹H NMR (400 MHz, CDCl₃): δ (ppm) 8.99 (s, 2H), 4.20–4.16 (t, 5H), 1.75–1.69 (m, 5H), 1.46–1.39 (m, 11H), 0.49–0.46 (m, 5H), 0.22–0.08 (m, 36H). ¹³C NMR (CDCl₃, 100 MHz): ppm 160.73, 160.70, 139.05, 128.30, 127.71, 125.35, 124.08, 41.59, 30.60, 27.66, 22.87, 17.55. Anal. Calc'd for C₃₈H₆₄Br₂N₂O₈Si₆: C, 45.40; H, 6.42; N, 2.79. Found: C, 45.11; H, 6.55; N, 2.67. MALDI-TOF MS: Calc'd for 1005.24. Found: 1007.31.

Synthesis of P(NDI2SiC₅-T2): Under argon, dibrominated monomer **1** (0.15 g, 0.149 mmol), bis-stannylated co-monomer T2 (150 mg, 0.149 mmol), Pd2(dba)₃ (2.1 mg), and tri-*o*-tolylphosphine (3.5 mg) were dissolved in anhydrous toluene (5 mL), stirred, and heated to 120 °C for 2 h. After cooling, the resulting polymer was precipitated into methanol (200 mL) and filtered off. The crude polymer was purified by Soxhlet extraction with methanol, acetone, hexane, and CF sequentially for the removal of low-molecular-weight product. This CF solution was re-precipitated in methanol. The precipitates were collected by filtration and dried in vacuum, leading to a dark greenish blue solid as the product (91 mg, yield 66.4%). ¹H NMR (400MHz, CDCl₃): δ (ppm) 8.83(m, 2H), 7.36–7.34 (m, 4H), 4.17–4.14 (m, 4H), 2.03–1.99 (m, 4H), 1.73–1.38 (br, 8H), 0.90–0.23 (br, 46H). Anal. Cal'd for C₄₆H₆₈N₂O₈S₂Si₆: C, 54.72; H, 6.79; N, 2.77. Found: C, 54.50; H, 6.74; N, 2.58. GPC data GPC: Mn = 4.7 KDa, Mw = 14.2 KDa, PDI = 3.02; the values represent only the parts that were soluble in THF.

Synthesis of P(NDI2SiC₅-TTh): P(NDI2SiC₅-TTh) was synthesized according to the same method as P(NDI2SiC₅-T2), except using bis-stannylated TTh (69.5 mg, 0.149 mmol) to replace T2 (90 mg, yield 61.5%) and reaction time (8 h). ¹H NMR (400MHz, CDCl₃): δ (ppm) 8.89 (m, 2H), 7.60-7.57 (m, 2H), 4.19–4.13 (m, 4H), 2.05–2.03 (m, 4H), 1.72–1.38 (br, 8H), 0.87–0.22 (br, 46H). Anal. Cal'd for C₄₄H₆₆N₂O₈S₂Si₆: C, 53.73; H, 6.76; N, 2.85. Found: C, 53.50; H, 6.80; N, 2.79. GPC: Mn = 12.5 KDa, Mw = 63.4 KDa, PDI = 5.05; the values represent only the parts that were soluble in THF.

Fabrication and characterization of OFETs: To investigate the effects of alkyl and hybrid siloxane side chains on the characteristics of n-channel OFETs, we fabricated top-gate,

bottom-contact (TG/BC) OFETs based on P(NDI2SiC₅-T2) and P(NDI2SiC₅-TTh). TG/BC structure OFETs were fabricated on Au/Ni electrode pre-patterned Corning Eagle 2000 glass substrates by spin coating of the semiconducting polymers. Au/Ni electrode patterned samples were cleaned sequentially in an ultrasonic bath with de-ionized water, acetone, and isopropanol for 10 min each and UV treated for 30 min. The polymer thin films (~35 nm thickness) were prepared by NDI polymer solution in CF (4 mg/mL) using the spin-coating method at 2000 rpm for 60 s, and then sequentially thermally annealed at 100, 200, and 300 °C for 30 min in a nitrogen (N₂)-filled glove box. The polymer also dissolved in other solvents: CN, DCB, and TCE at 4 mg/mL to check the solubility effect. Polymethylmethacrylate (PMMA) polymer dielectric layer was purchased from Sigma-Aldrich dissolved in n-butyl acetate (nBA) at 80 mg/mL. PMMA thin film was formed on a hybrid siloxane-NDI-bithiophene layer by spin coating followed by thermal baking at 80 °C for ~1 h in the same N₂-filled glove box to remove the residual solvents. The OFET device fabrication was completed by depositing the aluminum (Al) top-gate electrodes (~50 nm thick) via thermal evaporation using a metal shadow mask. The transport characteristics were measured in an N₂-filled glovebox.

To extract contact resistance of OFETs, we used Y-function method (YFM), a fast and precise alternative method for obtaining R_c with few single device. From the transfer characteristics of the OFETs, I_d in the linear regime can be described as in following equation:

$$I_d = \frac{W}{L} C_i (V_g - V_{Th}) \frac{\mu_0}{1 + \theta(V_g - V_{Th})} \times V_d$$

with C_i is the dielectric capacitance per unit area, and μ_0 is the low-field mobility. θ is the mobility attenuation factor, which consists of the extrinsic factors caused by the surface roughness and phonon scattering (θ_0) and contact resistance [$\theta^* = (W/L)\mu_0 C_i R_c$]. Assuming a constant R_c , the trans conductance (g_m) can be expressed as

$$g_m = \frac{\delta I_d}{\delta V_g} = \frac{W}{L} C_i \frac{\mu_0}{[1 + \theta(V_g - V_{Th})]^2} \times V_d$$

θ can be obtained by plotting $1/g_m^{1/2}$ versus V_g at a strong charge accumulation, where a linear behavior is obtained. Assuming that θ_0 is negligible, R_c can be calculated.

Acknowledgements

The research was supported by a National Research Foundation of Korea (NRF) grant funded by the Korea government (MSIP) (2015R1A2A1A10053397) and (2014K1A3A1A19066591), and Nano-Material Technology Development Program through the National Research Foundation of Korea (NRF) funded by the Ministry of Science, ICT and Future Planning (NRF-2014M3A7B4051749). GIWAXD

experiments at PLS-II 6D UNIST-PAL beamline and 9A beamline were supported in part by MEST, POSTECH, and UNIST UCRF.

Notes and references

- G. Lu, J. Blakesley, S. Himmelberger, P. Pingel, J. Frisch, I. Lieberwirth, I. Salzmann, M. Oehzelt, R. Di Pietro and A. Salleo, *Nat. Commun.*, 2013, **4**, 1588.
- S. G. Bucella, A. Luzio, E. Gann, L. Thomsen, C. R. McNeill, G. Pace, A. Perinot, Z. Chen, A. Facchetti and M. Caironi, *Nat. Commun.*, 2015, **6**.
- S. W. Yun, J. H. Kim, S. Shin, H. Yang, B. K. An, L. Yang and S. Y. Park, *Adv. Mater.*, 2012, **24**, 911-915.
- G. Kim, S.-J. Kang, G. K. Dutta, Y.-K. Han, T. J. Shin, Y.-Y. Noh and C. Yang, *J. Am. Chem. Soc.*, 2014, **136**, 9477-9483.
- J. Yao, C. Yu, Z. Liu, H. Luo, Y. Yang, G. Zhang and D. Zhang, *J. Am. Chem. Soc.*, 2015.
- J. Lee, A.-R. Han, J. Kim, Y. Kim, J. H. Oh and C. Yang, *J. Am. Chem. Soc.*, 2012, **134**, 20713-20721.
- A. Han, G. K. Dutta, J. Lee, H. R. Lee, S. M. Lee, H. Ahn, T. J. Shin, J. H. Oh and C. Yang, *Adv. Funct. Mater.*, 2015, **25**, 247-254.
- H. Yan, Z. Chen, Y. Zheng, C. Newman, J. R. Quinn, F. Dötz, M. Kastler and A. Facchetti, *Nature*, 2009, **457**, 679-686.
- X. Gao, C.-a. Di, Y. Hu, X. Yang, H. Fan, F. Zhang, Y. Liu, H. Li and D. Zhu, *J. Am. Chem. Soc.*, 2010, **132**, 3697-3699.
- L. E. Polander, S. P. Tiwari, L. Pandey, B. M. Seifried, Q. Zhang, S. Barlow, C. Risko, J.-L. Brédas, B. Kippelen and S. R. Marder, *Chem. Mater.*, 2011, **23**, 3408-3410.
- H. Zhong, J. Smith, S. Rossbauer, A. J. White, T. D. Anthopoulos and M. Heeney, *Adv. Mater.*, 2012, **24**, 3205-3211.
- A. Luzio, D. Fazzi, D. Natali, E. Giussani, K. J. Baeg, Z. Chen, Y. Y. Noh, A. Facchetti and M. Caironi, *Adv. Funct. Mater.*, 2014, **24**, 1151-1162.
- J. Chang, Q. Ye, K.-W. Huang, J. Zhang, Z.-K. Chen, J. Wu and C. Chi, *Org. Lett.*, 2012, **14**, 2964-2967.
- V. Lemaire, L. Muccioli, C. Zannoni, D. Beljonne, R. Lazzaroni, J. Cornil and Y. Olivier, *Macromolecules*, 2013, **46**, 8171-8178.
- A. Luzio, L. Criante, V. D'Innocenzo and M. Caironi, *Scientific Reports*, 2013, **3**.
- S. Fabiano, C. Musumeci, Z. Chen, A. Scandurra, H. Wang, Y. L. Loo, A. Facchetti and B. Pignataro, *Adv. Mater.*, 2012, **24**, 951-956.
- Z. Chen, H. Lemke, S. Albert-Seifried, M. Caironi, M. M. Nielsen, M. Heeney, W. Zhang, I. McCulloch and H. Sirringhaus, *Adv. Mater.*, 2010, **22**, 2371-2375.
- X. Zhan, A. Facchetti, S. Barlow, T. J. Marks, M. A. Ratner, M. R. Wasielewski and S. R. Marder, *Adv. Mater.*, 2011, **23**, 268-284.
- T. Sakanoue and H. Sirringhaus, *Nature materials*, 2010, **9**, 736-740.
- H. Usta, A. Facchetti and T. J. Marks, *Acc. Chem. Res.*, 2011, **44**, 501-510.
- J. Choi, K.-H. Kim, H. Yu, C. Lee, H. Kang, I. Song, Y. Kim, J. H. Oh and B. J. Kim, *Chem. Mater.*, 2015, **27**, 5230-5237.
- R. Kim, B. Kang, D. H. Sin, H. H. Choi, S.-K. Kwon, Y.-H. Kim and K. Cho, *Chem. Commun.*, 2015, **51**, 1524-1527.
- W. Y. Lee, J. H. Oh, S. L. Suraru, W. C. Chen, F. Würthner and Z. Bao, *Adv. Funct. Mater.*, 2011, **21**, 4173-4181.

24. T. Mondal, T. Sakurai, S. Yoneda, S. Seki and S. Ghosh, *Macromolecules*, 2015, **48**, 879-888.
25. Y. Kim, D. X. Long, J. Lee, G. Kim, T. J. Shin, K.-W. Nam, Y.-Y. Noh and C. Yang, *Macromolecules*, 2015, **48**, 5179-5187.
26. M. Stolte, M. Gsänger, R. Hofmockel, S.-L. Suraru and F. Würthner, *Phys. Chem. Chem. Phys.*, 2012, **14**, 14181-14185.
27. S. F. Völker, A. Schmiedel, M. Holzapfel, C. Böhm and C. Lambert, *Phys. Chem. Chem. Phys.*, 2013, **15**, 19831-19844.
28. S. Canola and F. Negri, *Phys. Chem. Chem. Phys.*, 2014, **16**, 21550-21558.
29. Y. Kim, J. Hong, J. H. Oh and C. Yang, *Chem. Mater.*, 2013, **25**, 3251-3259.
30. A. Facchetti, *Chem. Mater.*, 2010, **23**, 733-758.
31. J. Rivnay, R. Steyrlleuthner, L. H. Jimison, A. Casadei, Z. Chen, M. F. Toney, A. Facchetti, D. Neher and A. Salleo, *Macromolecules*, 2011, **44**, 5246-5255.
32. R. Steyrlleuthner, M. Schubert, I. Howard, B. Klaumünzer, K. Schilling, Z. Chen, P. Saalfrank, F. Laquai, A. Facchetti and D. Neher, *J. Am. Chem. Soc.*, 2012, **134**, 18303-18317.
33. R. Steyrlleuthner, R. Di Pietro, B. A. Collins, F. Polzer, S. Himmelberger, M. Schubert, Z. Chen, S. Zhang, A. Salleo and H. Ade, *J. Am. Chem. Soc.*, 2014, **136**, 4245-4256.
34. M. M. Szumilo, E. H. Gann, C. R. McNeill, V. Lemaure, Y. Oliver, L. Thomsen, Y. Vaynzof, M. Sommer and H. Sirringhaus, *Chem. Mater.*, 2014, **26**, 6796-6804.
35. D. Shukla, S. F. Nelson, D. C. Freeman, M. Rajeswaran, W. G. Ahearn, D. M. Meyer and J. T. Carey, *Chem. Mater.*, 2008, **20**, 7486-7491.
36. J. Lee, A.-R. Han, H. Yu, T. J. Shin, C. Yang and J. H. Oh, *J. Am. Chem. Soc.*, 2013, **135**, 9540-9547.
37. J. Lee, A. Han, S. M. Lee, D. Yoo, J. H. Oh and C. Yang, *Angew. Chem. Int. Ed.*, 2015, **54**, 4657-4660.
38. M. Caironi, C. Newman, J. Moore, D. Natali, H. Yan, A. Facchetti and H. Sirringhaus, *Appl. Phys. Lett.*, 2010, **96**, 3303.
39. Z. Chen, Y. Zheng, H. Yan and A. Facchetti, *J. Am. Chem. Soc.*, 2008, **131**, 8-9.
40. E. Giussani, D. Fazzi, L. Brambilla, M. Caironi and C. Castiglioni, *Macromolecules*, 2013, **46**, 2658-2670.
41. G.-J. A. Wetzelaer, M. Kuik, Y. Olivier, V. Lemaure, J. Cornil, S. Fabiano, M. A. Loi and P. W. Blom, *Phys. Rev. B*, 2012, **86**, 165203.
42. D. Khim, K.-J. Baeg, J. Kim, J.-S. Yeo, M. Kang, P. S. Amegadzea, M.-G. Kim, J. Cho, J. H. Lee and D.-Y. Kim, *J. Mater. Chem.*, 2012, **22**, 16979-16985.
43. K.-J. Baeg, J. Kim, D. Khim, M. Caironi, D.-Y. Kim, I.-K. You, J. R. Quinn, A. Facchetti and Y.-Y. Noh, *ACS Appl. Mater. Interfaces*, 2011, **3**, 3205-3214.
44. G. Dell'Erba, A. Luzio, D. Natali, J. Kim, D. Khim, D.-Y. Kim, Y.-Y. Noh and M. Caironi, *Appl. Phys. Lett.*, 2014, **104**, 153303.
45. C. Liu, Y. Xu and Y.-Y. Noh, *Mater. Today*, 2015, **18**, 79-96.
46. G. Greczynski, M. Fahlman and W. R. Salaneck, *J. Chem. Phys.*, 2001, **114**, 8628-8636.

TOC graphic only

